J. Fluid Mech. (1995), *vol.* 302, *pp.* 29–44

Evolution of a quasi-steady breaking wave

By J. C. LIN AND D. ROCKWELL

Department of Mechanical Engineering and Mechanics, Room 354, 19 Memorial Drive West, Lehigh University, Bethlehem, PA 18015, USA

(Received 5 January 1995 and in revised form 22 May 1995)

The stages of evolution of a quasi-steady breaker from the onset of a capillary pattern to a fully evolved breaking wave are characterized using high-image-density particle image velocimetry, which provides instantaneous representations of the free surface and the patterns of vorticity beneath it. The initial stage, which sets in at a low value of Froude number, involves a capillary pattern along each trough–crest surface of a quasi-stationary wave. The successive crests of the capillary pattern exhibit increasing scale and culminate in a single largest-scale crest of the free surface. Immediately upstream of the large-scale crest, the capillary pattern shows counterclockwise concentrations of vorticity at its troughs and regions of clockwise vorticity beneath its crests. The onset of the final, largest-scale crest exhibits two basic forms: one involving no flow separation; and the other exhibiting a small-scale separated mixing layer. At an intermediate value of Froude number, a breaker occurs and the capillary pattern is replaced by large-scale distortions of the free surface. The onset of separation, which involves flow deceleration along a region of the free surface having a large radius of curvature, leads to formation of a long mixing layer, which has substantial levels of vorticity. Downstream of this breaker, the long-wavelength wave pattern is suppressed. At the largest value of Froude number, the onset of flow separation rapidly occurs in conjunction with an abrupt change in slope of the surface, giving rise to vorticity concentrations in the mixing layer.

1. Introduction

Spilling breakers occur in a variety of free-surface systems, ranging from deep ocean waves to hydraulic jumps. Peregrine (1992) and Banner & Peregrine (1993) provide overviews of the principal features of these types of breakers. The onset of the breaking process involves relatively small-scale events in the form of capillary waves, as described by Longuet-Higgins (1973, 1990, 1992, 1994), whereas the final state of breaking exhibits irregular distortion of the free surface, in conjunction with large-scale separated flow beneath it, as addressed, for example, by Peregrine & Svendsen (1978) and Hoyt & Sellin (1989).

The initial stage of breaking of a short gravity wave, according to Longuet-Higgins (1992), involves the appearance of parasitic capillaries, which serve as a source of vorticity for the roller beneath the crest of the wave. The recent experiments of Duncan *et al.* (1994) show, for a propagating wave, that the initial train of capillaries is followed by a sequence of longer-wavelength capillaries, which exist above the toe of the bulge of the wave. On the basis of these observations, Longuet-Higgins (1994) proposes that the longer-wavelength capillaries are instability waves, which occur in a shear layer immediately beneath the free surface. The instability of a shear flow having a free-surface boundary on the upper side has received considerable attention over the past

two decades, as reviewed by Longuet-Higgins (1994). In fact, he demonstrates that the long-wavelength instabilities of Duncan *et al.* (1994) are well predicted by the model of Stern & Adam (1973). Furthermore, Longuet-Higgins proposes a simple model for these instabilities in terms of an array of discrete vortices, and shows that they should have a wavelength approximately four times that of the shorter-wavelength capillaries.

In contrast to these well-defined features of the initial stage of wave breaking, a fully evolved breaker exhibits large-scale, complex events. The final form of a spilling breaker is generally acknowledged to involve either a 'roller' near the crest of the wave or an extensive turbulent region beneath the free surface, or, in some interpretations, a combination of both. Hoyt & Sellin (1989) and Banner & Peregrine (1993) indicate the formation of an initial mixing-layer region, leading to a turbulent region beneath the wave crest, and Cointe & Tulin (1994) model a recirculating eddy sustained by turbulent stresses acting in the shear zone, i.e. mixing layer region. Lin & Rockwell (1994) provide images of the instantaneous, quantitative structure of a stationary wave undergoing breaking in the spilling mode. The breaker was fully evolved, in that the large change in slope at the onset of breaking occurred at the minimum elevation of the undisturbed free surface. At this location, rapid distortion of the flow along the free surface led to flow separation, in turn giving rise to a mixing layer with pronounced concentrations of vorticity.

In recent years, a wide range of investigations have addressed interactions of distributed and concentrated vorticity fields with a free surface. Certain features of these interactions are relevant to the processes of vorticity generation and free-surface distortion that may occur in a spilling breaker. Triantafyllou & Dimas (1989) and Dimas & Triantafyllou (1994) numerically simulated the linear and nonlinear interactions of a shear flow with a free surface in the absence of capillary effects. They describe the nonlinear evolution of two linearly unstable modes, which are dependent upon wavenumber and Froude number. The patterns of vortices formed beneath the crests and troughs of the free surface have distinctive features for each of the two modes; small deformations of the free-surface are related to the onset of breaking. For the case where the wavelength of the instability is long compared to the shear layer thickness, the unstable shear flow may be represented in terms of a submerged vortex street, as described by Tryggvason (1988) and Yu & Tryggvason (1990). Pronounced depressions of the free surface correspond to rollup of the vortex sheet; this scenario leads to a breaking wave. Interactions of coherent vorticity concentrations with a free surface include vortex pair configurations, which have been investigated experimentally by Sarpkaya & Henderson (1984) and Willmarth *et al.* (1989) and numerically by Ohring & Lugt (1989, 1991) and Lugt & Ohring (1992), as well as vortex rings, which have been addressed experimentally and numerically by Bernal & Kwon (1989) and Dommermuth & Yue (1991) respectively. Substantial and sharp distortions of the free surface are attainable for these classes of vortex–free-surface interactions and, as shown in the simulations of Ohring & Lugt (1991) and Lugt & Ohring (1992), opposite vorticity is generated from the local curvature of the surface, leading to formation of a secondary vortex.

For the case of a spilling breaker, pre-existing regions of distributed vorticity or vorticity concentrations need not be present in the region upstream of the breaker. Rather, the occurrence of regions of vorticity in conjunction with distortion of the free surface is an intrinsic feature of the self-generated process of wave breaking. The present investigation addresses the initial and intermediate stages of the breaking process, relative to the fully evolved state of wave breaking. A technique of high-image-density particle image velocimetry (PIV) allows insight into the instantaneous structure

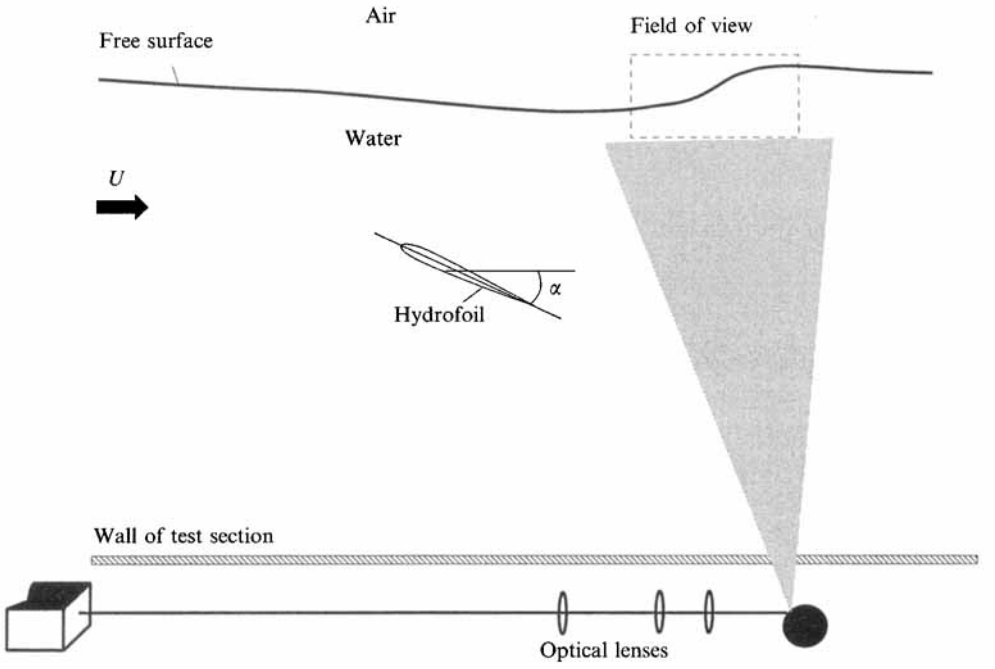

FIGURE 1. Overview of the experimental system illustrating the technique for the generation of quasi-steady breakers and the laser illumination for the high-image-density particle image velocimetry.

of these stages of breaking, in particular the instantaneous distributions of velocity and vorticity, relative to distortions of the free surface.

2. Experimental system and techniques

2.1. *Experimental system*

Experiments were performed in a free-surface water channel having an inlet width of 1828 mm and a depth of 584 mm. The flow passed through two successive contractions, each having an area ratio of 3:1, in order to optimize the quality of the flow in the test section, which had a width of 210 mm and a nominal water depth of 527 mm. The distance from the exit of the first contraction to the inlet of the second was 2100 mm. Each of the contractions gave a velocity deviation with the irrotational region of less than 1 %. A honeycomb-screen system was employed upstream of the first contraction in order to limit the turbulence intensity to less than 0.1 %.

The spilling breaker was generated by the hydrofoil free-surface configuration illustrated in figure 1. The general effectiveness of this approach has been thoroughly documented by Duncan (1981), Battjes & Sakai (1981), and Banner (1990). In the present experiments, a NACA 12 hydrofoil (airfoil) having a chord of 76 mm, and inclined at an angle of attack of $\alpha = 30°$, was located sufficiently far beneath the free surface such that a substantial region of irrotational flow existed between the wake of the hydrofoil and the free surface. A distance of 121 mm from the midcord of the hydrofoil to the free surface was found to more than satisfy this condition. The distance was determined by monitoring the far-field images showing the entire region of hydrofoil wake and the free surface while adjusting the height of the free

surface and the free-stream velocity. The flow velocity was varied over the range $334 \leqslant U \leqslant 482$ mm s^{-1}, corresponding to a range of Froude number Fr based on airfoil chord $0.39 \leqslant Fr \leqslant 0.56$.

The spilling breaker system is typically referred to as a quasi-steady or -stationary phenomenon, because significant fluctuations occur about an averaged or equilibrium state. The fact that such fluctuations are an inherent feature of the breaking process is underscored by the analyses of Banner (1988) and Cointe (1987). Banner (1988) considered global representations of the force system of the breaker, with the aim of predicting the perturbation response of the spilling zone. Extraneously induced perturbations of the free-surface region generated a response time of the breaker in accord with his model. Cointe (1987), following the work of Longuet-Higgins & Turner (1974), considered the entrainment of mass and momentum from the underlying wave, as well as shear stresses on the bottom of the breaker. The end result is the natural period of oscillation of the breaker, which is defined in dimensionless form as $T^* \equiv gT_{br}/2\pi c$, in which c is the equivalent phase speed of the stationary breaker and T_{br} is the period of the breaker oscillation. The experiments of Duncan (1981), involving a towed hydrofoil through quiescent water to generate the quasi-steady breaker, show good agreement with Cointe's (1987) theory, which predicts values of $T^* = 4$. For the present experimental conditions, the characteristic period of oscillation T_{br} was found to be approximately 0.66 s, giving values of the dimensionless parameter T^* in the range $4.89 \leqslant T^* \leqslant 6.12$. In view of this inherent unsteadiness about the equilibrium state of the breaker, it is essential that a whole-field instantaneous technique be employed for characterizing the velocity field at a given instant, allowing unambiguous definition of the instantaneous states of the breaker. The experimental approach employed herein satisfies this requirement.

2.2. *Experimental techniques*

In order to determine the instantaneous velocity field beneath the free surface, high-image-density particle image velocimetry was employed. A scanning laser version of this technique, described by Rockwell *et al.* (1993) allowed, in effect, generation of pulsed sheets of laser light by high-speed scanning of the beam across the plane of interest. This approach illuminates each particle of the flow with the full intensity of the laser beam during each sweep. In order to optimize the magnification of the image acquisition, a high-intensity (26 W) continuous-wave Argon-ion laser (Coherent Innova) was employed. The beam from this laser passed through a series of beam conditioning optics, then impinged upon a rotating mirror having 72 facets. The scanning frequency of the beam generated using this approach was 3000 cycles per second, which provided the desired spacing between successive images of each particle. In order to generate particle images that could be recorded by the camera, the flow was seeded with 12 μm, metallic-coated particles. The shutter of the 35 mm camera was opened long enough during each exposure such that six images of each particle were typically recorded on the film. Use of a rotating bias mirror in front of the camera lens imparted a constant bias velocity in the vertical direction to the pattern of particle images. This procedure precluded difficulties associated with large dynamic range and directional ambiguity in regions of flow separation. The mirror rotated at a sufficiently high rate to induce a bias velocity of 480 mm s^{-1}. Particle images were recorded on film having a resolution of 300 lines mm^{-1}, with a lens magnification of 1:2. This magnification gave a field of view 70 mm long in the physical plane of the laser sheet. The length of each of the images shown in figures 5 and 6 is 68 mm.

In order to determine the instantaneous velocity field corresponding to the pattern

of particle images, each image was digitized at a resolution of 125 pixels mm^{-1}. At each interrogation location on the negative, the velocity vector was determined using a single-frame cross-correlation approach based on the concept of Meinhart, Prasad & Adrian (1992). The size of the interrogation window was generally 0.72 mm × 0.72 mm, but was decreased to 0.51 mm × 0.51 mm in regions where higher resolution was desirable. A 50% overlap was maintained, in accord with the Nyquist criterion. As a consequence, the minimum grid size was 0.255 mm, corresponding to 0.51 mm in the plane of the laser sheet. This approach yielded approximately 2000 to 4000 velocity vectors in each image.

In addition to this quantitative approach, qualitative flow visualization was carried out during preliminary diagnostics of the wave patterns. A large number of multiply exposed images were recorded on each frame of a high-resolution video camera (1.1 megapixels). This technique was particularly insightful for relating the capillary wave patterns to the flow structure beneath them.

Crucial to interpretation of the free-surface distortion and the velocity and vorticity fields beneath it is proper definition of the free surface. This was accomplished by enlarging sections of the digitized image with a magnification of approximately 35:1, and digitizing the coordinates of the free surface using a cursor technique. Using this approach, the uncertainty in specifying the surface location was estimated to be ± 0.3 mm in the physical plane of the laser sheet, which is adequate resolution for defining the distorted free surface, except for the regions of small curvature at steep wave troughs. Furthermore, during experiments, proper orientation of the line of sight of the camera lens relative to the free surface is necessary in order to provide an unambiguous representation of the free-surface coordinates. Extensive preliminary studies showed that an angle of inclination of the axis of the camera lens of 18° with respect to the free surface ensured that certain regions of the surface were not obscured. In order to convert the digitized particle displacements and thereby the velocity vectors to values corresponding to an equivalent plane oriented orthogonally to the axis of the camera lens, a transformation function was employed.

3. Distortions of the free surface

Figure 2 shows representative instantaneous shapes of the free surface as a function of Froude number Fr. In view of the fact that the breaking process is inherently unsteady, as described in the preceding section, each of the instantaneous states of the free surface shown in figure 2 must be taken as a nominal state, about which time-dependent distortions can occur.

At the lowest speed, corresponding to $Fr = 0.39$, the free surface is undisturbed, exhibiting a single broad crest at the right side of the image. At a larger value of Froude number, $0.41 \leqslant Fr \leqslant 0.45$, the trough–crest surface of interest was actually the first in a quasi-stationary wave pattern having a wavelength of approximately 100 mm. In this range, well-defined small-scale distortions of the free surface are detectable. At $Fr = 0.43$, represented in figure 2, the free surface at the left side of the image is horizontal and relatively undisturbed. This quiescent zone is followed by a capillary pattern having small-scale, then larger-scale, crests eventually culminating in a single large-scale crest, which appears at essentially the same streamwise location as the broad crest of the undisturbed surface at $Fr = 0.39$. This capillary pattern at $Fr = 0.43$ has wavelengths ranging from 2 to 7 mm. Its form and wavelength range are similar to the patterns depicted by Longuet-Higgins (1992, 1994).

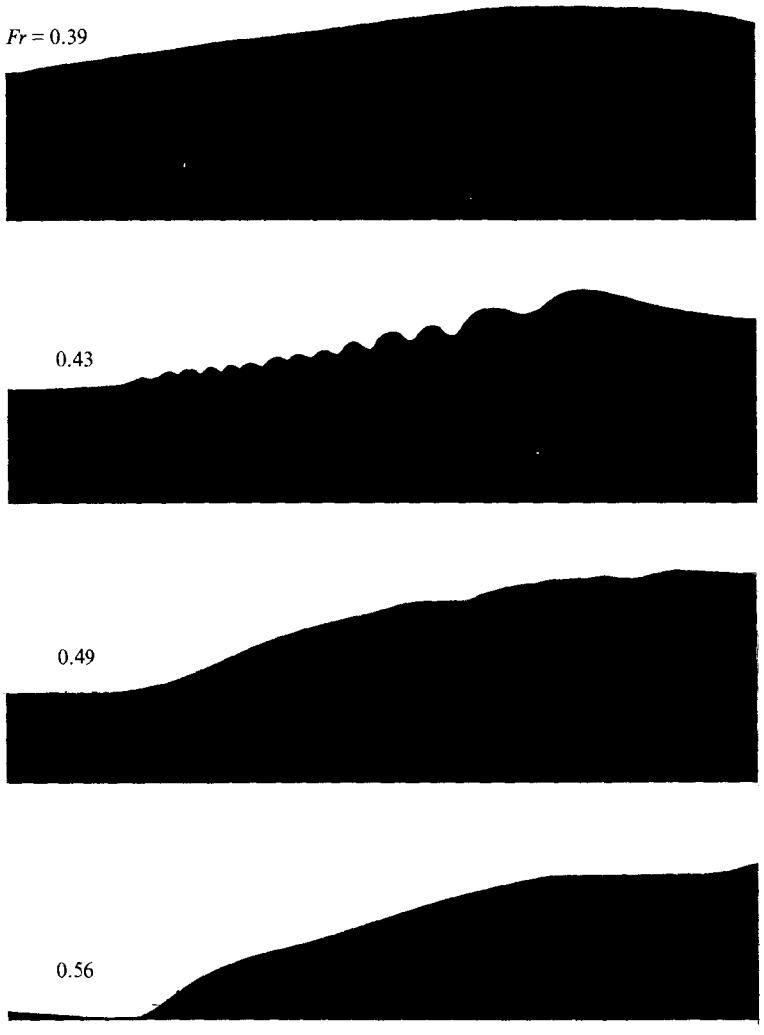

FIGURE 2. Basic classes of instantaneous free-surface distortion as a function of Froude number Fr based on chord of hydrofoil. Actual length of each image is 68 mm.

Further increase of the Froude number to $Fr = 0.49$ generates an abrupt change in the free-surface pattern. It now exhibits a concave shape with large radius in the region where the surface undergoes an initial increase in elevation; this region is followed by irregular distortions of the free surface up to the crest, due to existence of a zone of separated flow beneath the surface. A small-scale capillary pattern exists, however, over the region of the free surface immediately upstream of the onset of breaking. The wavelength between capillary crests is of the order of 1 mm and the pattern extends over a distance of 12 mm. Resolution of the detailed structure of this capillary was not attainable, and it is therefore not shown in figure 2. This free-surface pattern at $Fr = 0.49$ does not exist on each trough–crest surface of a successive long-wavelength quasi-stationary wave pattern, as is the case for the lower-Fr regime described in the foregoing. Downstream of the breaker, crest amplitudes are suppressed in a fashion similar to that modelled by Cointe & Tulin (1994).

An increase to a value of $Fr = 0.56$ produces a final transformation of the free

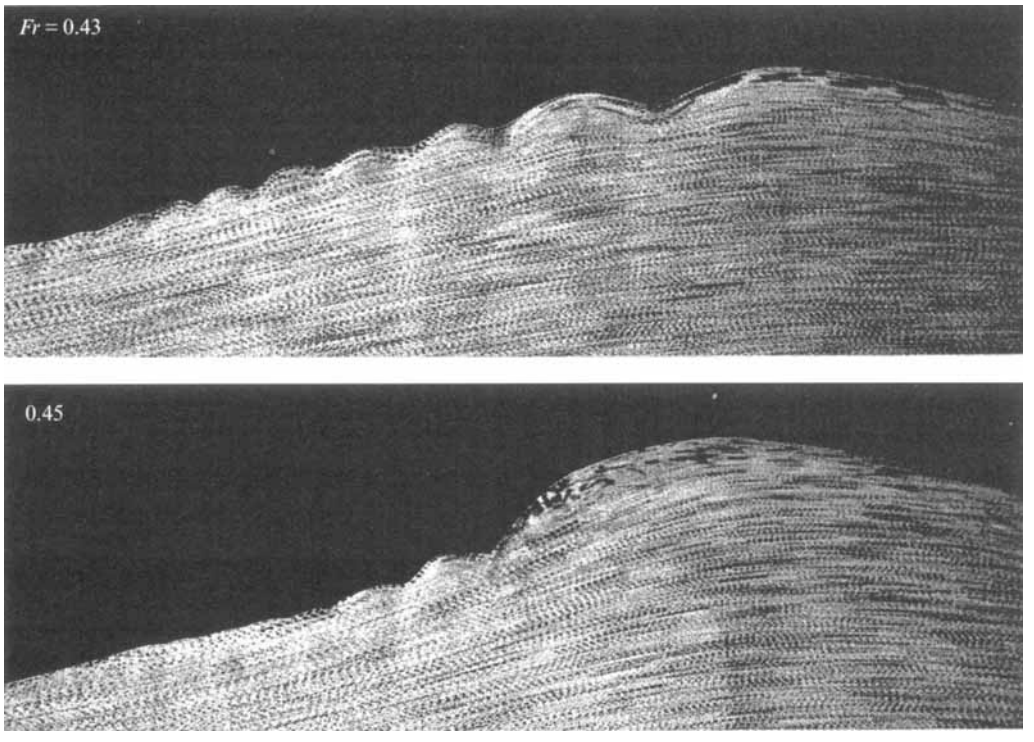

FIGURE 3. Digitized frames of multiply exposed images of 12 μm particles beneath capillary patterns at values of Froude number $Fr = 0.43$ and 0.45, illustrating the extreme sensitivity of the patterns. Actual length of each image is 47 mm.

surface such that a so-called fully evolved breaker occurs. In this case, the toe of the breaker is coincident with the minimum elevation of the free surface. An abrupt change in slope of the surface is evident at the onset of breaking, accompanied by a sudden increase in elevation. In this case, very small capillary waves having a wavelength of less than 1 mm exist over an extent of approximately 6 mm immediately upstream of the onset of breaking.

An intriguing feature of the free-surface patterns of figure 2 is that the well-defined capillary pattern at $Fr = 0.43$ occurs over a narrow band of Fr. Slightly decreasing or increasing Fr completely transforms this pattern. In order to demonstrate its sensitivity within a narrow band of Fr, images were acquired at two closely spaced values, as shown in figure 3. These images were obtained by generating a much larger number of multiple exposures of each particle than for quantitative measurements using the high-image-density PIV technique. At $Fr = 0.43$, the configuration of the capillary pattern is very similar to that of figure 2. Separation occurs beneath neither the entire succession of capillary crests nor the final largest scale crest. A slight increase to $Fr = 0.45$ generates a decrease in the number of capillary crests and troughs, steepening of the final capillary trough, and onset of flow separation involving the formation of a small-scale mixing layer beneath the final large-scale crest. These patterns at $Fr = 0.43$ and 0.45 are metastable. Self-excited transformation from one to the other could be observed.

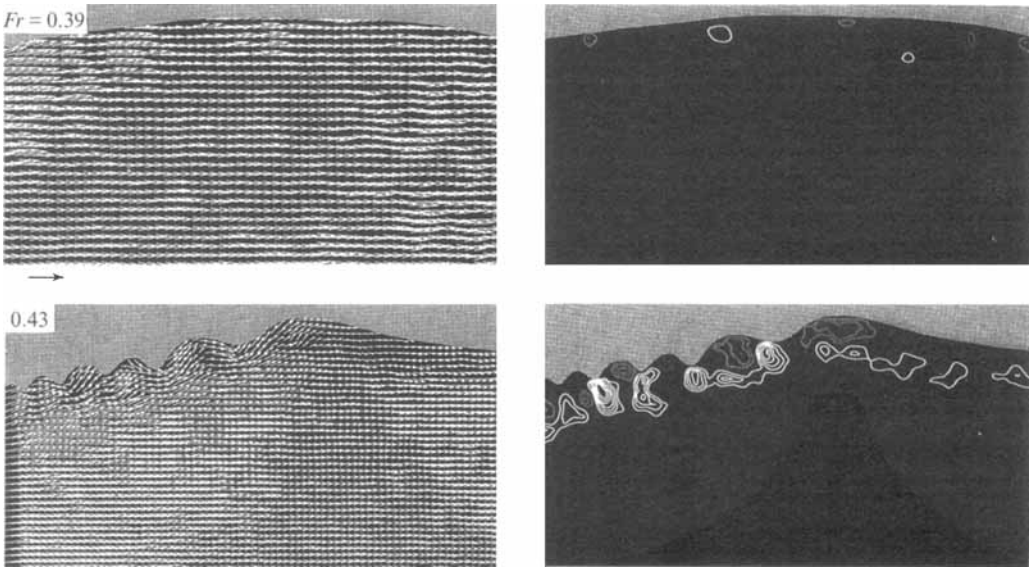

FIGURE 4. Images of instantaneous velocity and vorticity at $Fr = 0.39$ and 0.43, corresponding respectively to the cases of an undisturbed free surface and a capillary wave pattern along the surface. Minimum and incremental levels of vorticity are $|\omega_{min}| = 60\ s^{-1}$ and $\Delta\omega = 40\ s^{-1}$. The vector below each velocity image corresponds to 334 mm s^{-1} and 369 mm s^{-1} at $Fr = 0.39$ and 0.43, respectively. Actual length of each image is 37 mm.

4. Patterns of instantaneous velocity and vorticity

Instantaneous distributions of velocity and positive (white) and negative (grey) vorticity are shown for the two lowest values of $Fr = 0.39$ and 0.43 in figure 4. The field of view of these images corresponds approximately to the upper right half of the free-surface images shown in figure 2. The upper set of images of figure 4, corresponding to $Fr = 0.39$, shows uneventful distributions of velocity and insignificant levels of vorticity. At $Fr = 0.43$, represented by the bottom set of images, the velocity field in the laboratory frame shows that no significant regions of flow separation occur beneath either the three longer-wavelength capillary crests or, more importantly, beneath the final crest. We therefore conclude that the transformation of the free surface, starting with the capillary pattern of small-scale, then larger-scale, crests and culminating in a final crest, can be accomplished without separation of flow beneath the surface.

The corresponding vorticity contours show pronounced concentrations of positive (white) vorticity at the capillary troughs having longer wavelengths. In addition, regions of negative (grey) vorticity are indicated beneath two of the large-scale crests, as well as beneath the final crest. It should be emphasized, however, that the raw vorticity plot having a lower threshold value indicates negative vorticity beneath all crests; for clarity, a higher threshold value was employed for the plot of figure 4. This alternating sign of the vorticity is in general according with that predicted by Longuet-Higgins (1992) for the shapes of pure capillary waves corresponding to Crapper's (1957) solution. The calculations of Longuet-Higgins (1992) for the vorticity generated at the surface of such a capillary wave pattern suggests that the maximum vorticity at the trough will be much larger than that at the crest for the height h to wavelength λ ratios, i.e. h/λ, characteristic of the pattern in figure 4. Indeed, the positive (white) concentrations generally exhibit maximum values of vorticity of the order of three times that of the negative (grey) regions. Of course, the inherent unsteadiness of the

capillary system may distort somewhat both the level and form of the regions of vorticity shown in figure 4.

The concentrations of positive (white) vorticity at the troughs of the capillary pattern have values of circulation $\Gamma^* = \Gamma/2\pi U\lambda_v$ in the range of 0.11 to 0.19; U is the free-stream velocity and λ_v is the average wavelength between concentrations. On the other hand, negative (grey) regions of vorticity have values extending from $\Gamma^* = 0.01$ to 0.08. Regarding the region of negative vorticity beneath the final crest of the pattern in figure 4, it has a sense compatible with the free-surface curvature of the crest, but opposite to that typically hypothesized as a recirculation vortex or roller beneath the crest. Low-level positive (white) vorticity concentrations, evident in the region downstream of the final trough, may be due to shedding of vorticity from the perturbed capillary.

At higher values of Fr, as shown in figure 2, the well-defined capillary pattern gives way to an irregularly distorted surface, below which separation occurs. Two representative values of $Fr = 0.49$ and 0.56, corresponding to intermediate and fully evolved stages of breaking, are shown in the images of figures 5 and 6. In figure 5, the top two images correspond to $Fr = 0.49$ and 0.56 respectively, and the instantaneous velocity field beneath the free surface is shown in a reference frame moving to the left at a speed equal to two-thirds the inflow velocity. This representation highlights the extent of the separated zone beneath the wave, corresponding to the high-density long-length velocity vectors pointing to the left. It also allows identification of the onset of separation from the free surface. At $Fr = 0.49$, separation occurs from a region of large radius of curvature and at a location above the minimum elevation of the free surface. On the other hand, at $Fr = 0.56$, it occurs from a region of the free surface exhibiting an abrupt change in slope, which is coincident with the minimum elevation of the surface. Moreover, we note that the image at $Fr = 0.49$ shows a sink-type behaviour at the separation point, i.e. vectors from upstream and downstream regions point to the same location on the free surface. On the other hand, at $Fr = 0.56$, the onset of separation occurs at a location of oppositely directed vectors adjacent to the surface. The detailed structure of this separation region at higher resolution will be addressed subsequently.

The bottom set of images in figure 5 corresponds to a reference frame moving to the left at one-third the inflow velocity. They indicate the large-scale vortical activity in the mixing layer arising from separation from the free surface. At both values of Fr, swirl patterns of velocity vectors are evident in this layer. At the higher value $Fr = 0.56$, closed swirl patterns are particularly well-defined, even in regions close to the onset of separation. Apparently, the rapid distortion of the flow in the vicinty of separation from the abrupt change in slope of the free surface promotes more rapid formation of vortical structures at this Froude number. Video records revealed that the swirl patterns can grow intermittently to even larger scales as they evolve downstream, giving rise to well-defined distortions of the free surface. These surface distortions were directly linked to the wavelength between the large-scale vortical structures.

The top two images of figure 6 show the velocity field in the laboratory reference frame. This representation emphasizes the large-scale vortical motion in the mixing-layer region in conjunction with the low-velocity turbulent region beneath the free surface. At the lower value of $Fr = 0.49$, this turbulent low-velocity region has a relatively small height. At $Fr = 0.56$, however, its height increases substantially in accord with the severe change in slope and abrupt increase in elevation of the free surface at the onset of separation. At neither $Fr = 0.49$ nor 0.56 is there any indication of a large-scale pattern of velocity vectors, which would suggest the existence of a

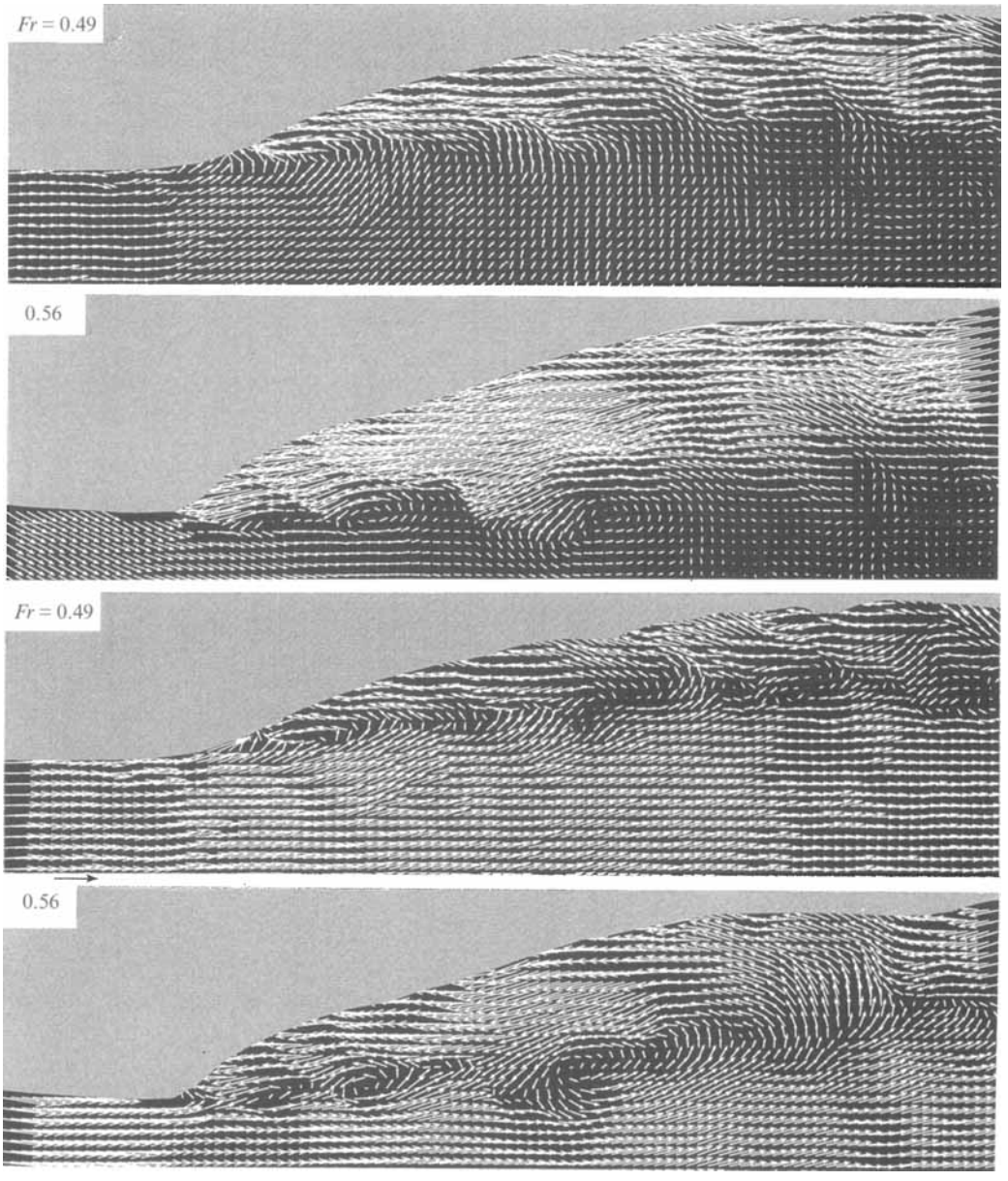

FIGURE 5. Images of instantaneous velocity for a breaker in the intermediate ($Fr = 0.49$) and fully evolved ($Fr = 0.56$) states. The upper two images correspond to a reference frame moving to the left at a velocity equal to two-thirds the inflow velocity; the bottom two images are in a frame moving at one-third the inflow velocity. Vectors below velocity images at $Fr = 0.49$ and 0.56 represent velocities of 422 and 482 mm s^{-1} respectively. Actual length of each image is 64 mm.

recirculation vortex having closed streamlines, located beneath the free surface, and extending from the onset of separation to a location well downstream of it. The mid-portion of this image at $Fr = 0.56$ does suggest a localized region of recirculation; it is associated with a large-scale cluster of vorticity in the mixing layer. In order to establish whether a so-called recirculation zone exists along the entire extent of the

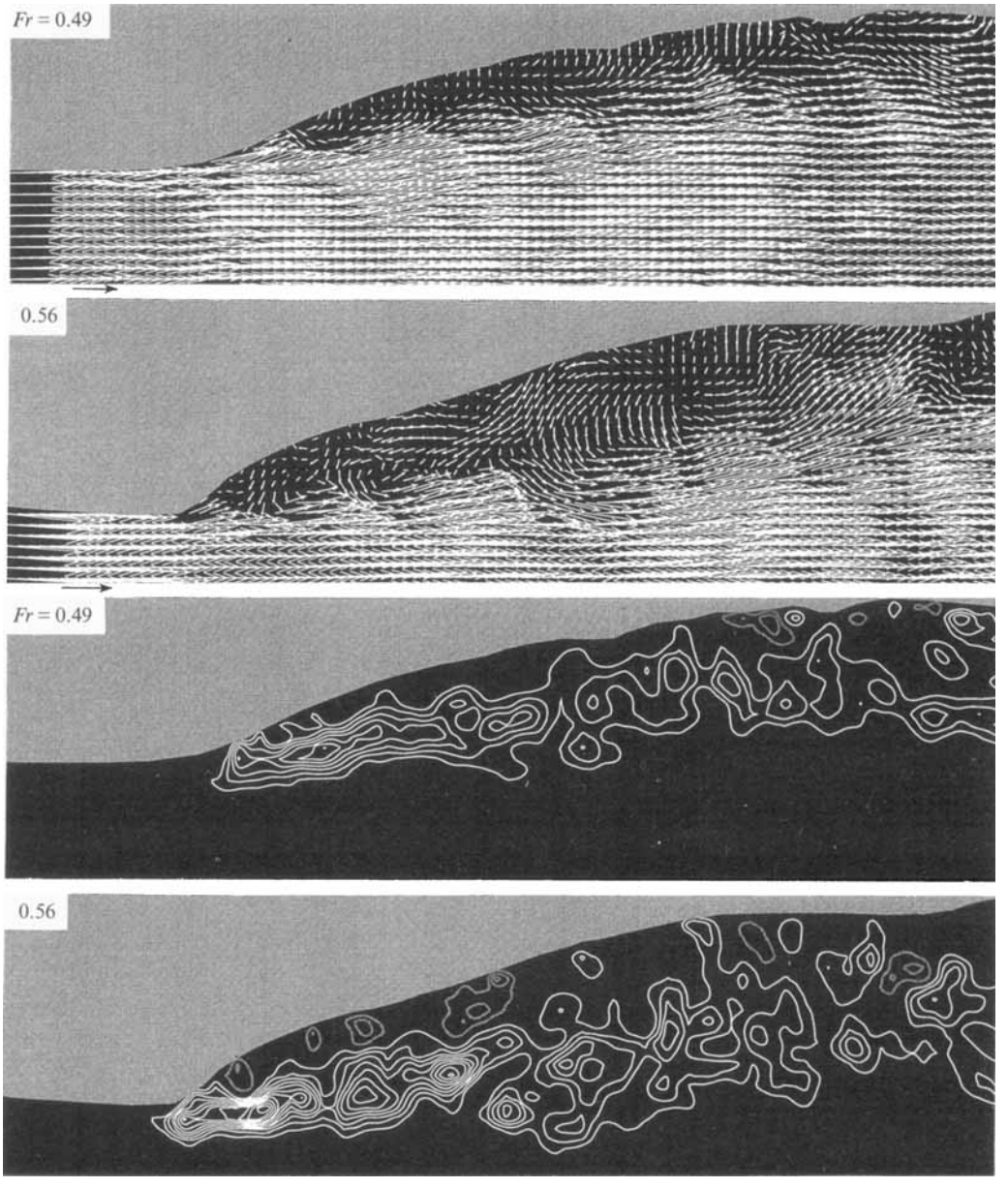

FIGURE 6. Comparison of instantaneous velocity distributions in laboratory (fixed) frame and contours of constant positive (white) and negative (grey) vorticity for a breaker in intermediate ($Fr = 0.49$) and fully evolved ($Fr = 0.56$) states. The scale of velocities is the same as for figure 5. Minimum and incremental levels of vorticity are $|\omega_{min}| = 40\ s^{-1}$ and $\Delta\omega = 40\ s^{-1}$. Actual length of all images is 64 mm.

breaker, it is necessary to time-average a number of instantaneous images; the substantial fluctuations of the free surface, however, make it difficult to secure a meaningful average.

Corresponding contours of constant vorticity are shown in the bottom set of images of figure 6. At both $Fr = 0.49$ and 0.56, the maximum levels of vorticity, $\omega_{max} = 282\ s^{-1}$ and $456\ s^{-1}$ respectively, occur in the region of intense shear immediately downstream

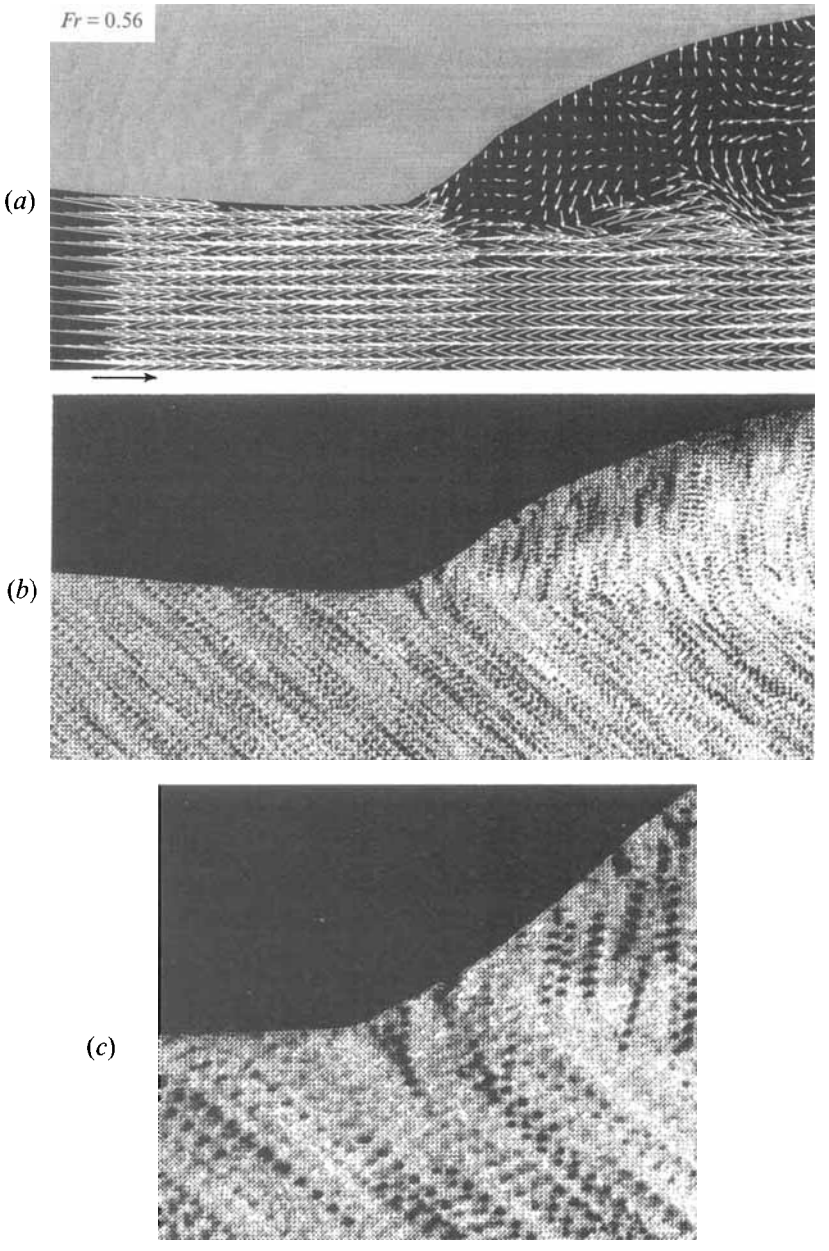

FIGURE 7. Close-up view of (*a*) instantaneous velocity distribution and (*b*, *c*) patterns of particle images at the onset of separation associated with fully evolved wave breaking ($Fr = 0.56$). The distance between particle images in (*c*) is approximately 100–200 microns. The vector below image (*a*) corresponds to 482 mm s^{-1}. Actual length of images (*a*) and (*b*) is 28 mm; actual length of (*c*) is 6 mm.

of the separation from the free surface. Although the velocity increases by only a factor of 1.14 in going from $Fr = 0.49$ to 0.56, the normalized maximum vorticity $\omega_{\max}$ increases by a factor of 2. This observation suggests that the detailed distortion of the flow adjacent to the free surface during the onset and development of flow separation, in conjunction with the change in slope of the free surface, plays a central role in determining the maximum vorticity ω_{max}.

Furthermore, the structure of the initially formed mixing layer, represented by the patterns of vorticity contours, is markedly different at the two values of Fr. At $Fr = 0.56$, pronounced concentrations of vorticity are immediately evident, and these have an average value of circulation $\Gamma_a/\pi U\lambda_v = 0.328$ and a maximum value of $\Gamma_{max}/\pi U\lambda_v = 0.523$. On the other hand, at $Fr = 0.49$, only an elongated concentration of vorticity is detectable immediately downstream of separation.

In order to gain further insight into the region of flow separation at $Fr = 0.56$, higher-resolution image processing was undertaken, corresponding to the smaller size of the interrogation window described in §2.2. The images of figure 7 represent the instantaneous velocity field and corresponding patterns of multiply exposed particle images. The velocity distribution of figure 7(*a*) shows that the magnitude of the velocity is virtually unaltered until the abrupt change in slope of the free surface is encountered. At this location, there is a rapid reduction in magnitude of the velocity. This change in the velocity field, which is accompanied by a sudden increase in elevation of the free surface, represents the transformation from an undisturbed, essentially uniform velocity field to a very low-velocity separated region beneath the free surface.

The pattern of particle images shown in figure 7(*b*) illustrates the large change in velocity across the separated layer formed from the curved free surface. In this image, approximately 4–6 multiply exposed images of each particle are shown. The bias velocity imposed by the rotating mirror is in the vertical direction; therefore in regions of very low velocity, the clusters of successive particle images are nearly vertical. On the other hand, in the free-stream region, where the horizontal component of velocity is of the same order as the vertical bias velocity, the patterns of images are inclined at approximately 45° to the horizontal. The abrupt change in slope of these patterns of particle images is evident along a horizontal line emanating from the onset of separation at the free surface.

More insightful, however, is the zoom view shown in figure 7(*c*). The length of the entire image corresponds to only 6 mm in the actual flow; the distance between neighbouring particle images is of the order of 100–200 μm. Near the region of the free-surface having a small radius of curvature, the pattern of images undergoes a drastic change in slope over a very small streamwise distance of about 300 μm. It corresponds to a sudden drop in the value of streamwise velocity. We therefore see that the process of flow separation involves a substantial reduction in velocity over a remarkably small streamwise distance along the free surface.

5. Concluding remarks

The initial stage of development of a spilling breaker involves formation of a capillary pattern upstream of the crest of the stationary wave. It exhibits a train of small-scale, then larger-scale, crests similar to the patterns suggested by Longuet-Higgins (1992, 1994) and by Duncan *et al.* (1994) based on free-surface visualization of a propagating wave. The maximum value of circulation is $\Gamma^*_{max} \equiv \Gamma_{max}/\pi U\lambda_v \approx 0.2$ for concentrations of vorticity formed at the troughs of the capillary pattern. For the range of parameters investigated, flow separation did not occur beneath the capillary troughs and crests; however, there is a source of vorticity creation due to curvature of the free surface, as described by Longuet-Higgins (1994). This state of non-separated flow beneath the crests of the capillary pattern of successively increasing wavelength is a delicate one. Either very small changes in Froude number or self-excited, unsteady distortions of the free surface can sharpen the final trough of the capillary pattern, thereby generating a separated zone beneath the enlarged final crest of the wave.

At larger values of Froude number, the wavelength of the capillary pattern decreases to less than a millimetre. This pattern is confined to a small region immediately upstream of the onset of flow separation. The distortion of the flow along the free surface during the onset of separation, in accord with the change in slope of the surface, leads to a large-scale mixing layer. Within this layer, identifiable concentrations of vorticity have a maximum value of circulation of the order of $\Gamma^*_{max} = 0.5$ at $Fr = 0.56$. These concentrations occur following separation from a region of the free surface having a severe change in slope. In fact, close ups of the instantaneous velocity field in this region show that the sudden onset of flow separation occurs in a very localized region where the free surface undergoes an abrupt increase in elevation. At the onset of separation, the component of velocity immediately beneath the free surface shows a severe decrease. This rapid distortion of the near-surface velocity field is associated with high levels of vorticity in the mixing layer formed immediately downstream of it. In fact, values as high as $\omega_{max} = 400\ s^{-1}$ are attainable in this region. The detailed structure of the region of flow separation from the free surface is hypothesized to be important in determining the magnitude of the vorticity in the mixing layer. In fact, wave breaking at a Froude number $Fr = 0.49$, lower than the value of $Fr = 0.56$ corresponding to the fully evolved breaker, exhibits a large radius of curvature of the free surface, and the details of the flow separation process are altered accordingly. In this case, the maximum value of vorticity is of the order of $\omega_{max} = 180\ s^{-1}$ and no pronounced concentrations of vorticity are evident in the mixing layer immediately downstream of separation.

In summary, evolution of the breaker from a small-scale capillary pattern to a large-scale separated region beneath an irregularly distorted free surface occurs over a relatively narrow range of Froude number. Each of the individual states identified within this range is a delicate one, in that self-excited distortions can occur. Each state is, however, generally identifiable and can be classified on the basis of Froude number. Two distinctly different mechanisms give rise to regions of concentrated vorticity: one involves non-separated flow about the curved troughs and crests of the capillary pattern; and the other flow separation from the curved free surface of the large-scale breaker. In regions where the radius of curvature of the free surface is small and the flow remains attched to the surface, well-defined concentrations of vorticity exist, i.e. flow beneath the train of capillary patterns leads to quasi-stationary vorticity concentrations beneath their troughs. At the other extreme, for the fully evolved breaker, convecting vorticity concentrations arise from disturbance amplification in the mixing layer formed by flow separation from the free surface; they move downstream in the mixing layer at a fraction of the free-stream velocity. Despite the fundamental differences in the origin and physical features of the capillary pattern and the fully evolved breaker, the maximum value of circulation Γ^* of the vorticity concentrations in both of these systems is the same order of magnitude, the latter being only about twice the former.

Further consideration of this class of flows should assess the three-dimensionality of the breaking process, in particular the spanwise structure of the vortical structures formed in the separated shear layer generated at the onset of breaking. Such an effort is planned in our laboratory.

The authors gratefully acknowledge support of the Office of Naval Research (Grant N00014-94-1-0185).

REFERENCES

BANNER, M. L. 1988 Surging characteristics of spilling zones of quasi-steady breaking water waves. *Proc. IUTAM Symp. on Nonlinear Waterwaves, 1987, Tokyo, Japan* (ed. K. Horikawa & H. Maruo). Springer.

BANNER, M. L. 1990 The influence of wave breaking on the surface pressure distribution in wind–wave interactions. *J. Fluid Mech.* **211**, 463–495.

BANNER, M. L. & PEREGRINE, D. H. 1993 Wave breaking in deep water. *Ann. Rev. Fluid Mech.* **25**, 373–397.

BATTJES, J. A. & SAKAI, T. 1981 Velocity field in a steady breaker. *J. Fluid Mech.* **111**, 421–438.

BERNAL, L. P. & KWON, J. T. 1989 Vortex ring dynamics at a free surface. *Phys. Fluids* A **1**, 1–61.

COINTE, R. 1987 A theory of breakers and breaking waves. PhD dissertation, University of California, Santa Barbara (University Microfilms Order No. 8811824).

COINTE, R. & TULIN, M. P. 1994 A theory of steady breakers. *J. Fluid Mech.* **276**, 1–20.

CRAPPER, G. D. 1957 An exact solution for progressive capillary waves of arbitrary amplitude. *J. Fluid Mech.* **2**, 532–540.

DIMAS, A. A. & TRIANTAFYLLOU, G. S. 1994 Nonlinear interaction of shear flow with a free surface'. *J. Fluid Mech.* **260**, 211–246.

DOMMERMUTH, D. C. & YUE, D. K. P. 1991 A numerical study of three-dimensional viscous interactions of vortices with a free surface. In *Eighteenth Symp. on Naval Hydrodynamics, University of Michigan, Ann Arbor*, pp. 727–788.

DUNCAN, J. H. 1981 An experimental investigation of breaking waves produced by a towed hydrofoil. *Proc. R. Soc. Lond.* A **377**, 331–348.

DUNCAN, J. H., PHILOMIN, V., BEHRES, M. & KIMMEL, J. 1994 The formation of spilling breaking water waves. *Phys. Fluids* **6**, 2558–2560.

HOYT, J. W. & SELLIN, R. H. T. 1989 The hydraulic jump as a mixing layer. *J. Hydraul. Div. ASCE* **115**, 1607–1614.

LIN, J.-C. & ROCKWELL, D. 1994 Instantaneous structure of a breaking wave. *Phys. Fluids* **6**, 2877–2879.

LONGUET-HIGGINS, M. S. 1973 A model of flow separation at a free surface. *J. Fluid Mech.* **57**, 129–148.

LONGUET-HIGGINS, M. S. 1990 Flow separation near the crests of short gravity waves. *J. Phys. Oceanogr.* **20**, 595–599.

LONGUET-HIGGINS, M. S. 1992 Capillary rollers and bores. *J. Fluid Mech.* **240**, 659–679.

LONGUET-HIGGINS, M. S. 1994 Shear instability in spilling breakers. *Proc. R. Soc. Lond.* A **446**, 399–409.

LONGUET-HIGGINS, M. S. & TURNER, J. S. 1974 An 'entraining plume' model of a spilling breaker. *J. Fluid Mech.* **63**, 1–20.

LUGT, H. J. & OHRING, S. 1992 The oblique ascent of a viscous vortex pair toward a free-surface. *J. Fluid Mech.* **236**, 461–476.

MEINHART, C. D., PRASAD, A. K. & ADRIAN, R. J. 1992 Parallel digital processor system for particle image velocimetry, *Sixth Intl Symp. on Applications of Laser Techniques to Fluid Mechanics, Lisbon, Portugal, July 20–30*, pp. 30.1.1 to 30.1.5.

OHRING, S. & LUGT, H. J. 1989 Two counter-rotating vortices approaching a free surface in a viscous fluid. *David Taylor Research Center Rep.* DTRC-89/013.

OHRING, S. & LUGT, H. J. 1991 Interaction of a viscous vortex pair with a free surface. *J. Fluid Mech.* **227**, 47–70.

PEREGRINE, D. H. 1992 Mechanisms of wave breaking. In *Proc. IUTAM Symp. on Breaking Waves* (ed. M. L. Banner & R. H. J. Grimshaw). Springer.

PEREGRINE, D. H. & SVENDSEN, I. A. 1978 Spilling breakers, bores and hydraulic jumps. *Proc. Sixteenth Conf. on Coastal Engineering*, pp. 540–550. ASCE.

ROCKWELL, D., MAGNESS, C., TOWFIGHI, J., AKIN, O. & CORCORAN, T. 1993 High-image-density particle image velocimetry using laser scanning techniques. *Exps. Fluids* **14**, 181–192.

SARPKAYA, T. & HENDERSON, D. O. 1984 Surface disturbances due to trailing vortices. *Naval Postgraduate School, Monterey, California, Rep.* NPS-69-84-004.

STERN, M. E. & ADAM, Y. A. 1973 Capillary waves generated by a shear current in water. *Mem. Soc. R. Sci. Liège* **6**, 179–185.

TRIANTAFYLLOU, G. S. & DIMAS, A. A. 1989 Interaction of two-dimensional separated flows with a free surface at low Froude numbers. *Phys. Fluids* A, **1**, 1813–1821.

TRYGGVASON, G. 1988 Deformation of a free surface as a result of vortical flows. *Phys. Fluids* **31**, 955–957.

WILLMARTH, W. W., TRYGGVASON, G., HIRSA, A. & YU, D. 1989 Vortex pair generation and interaction with a free surface. *Phys. Fluids* A **1**, 170–172.

YU, D. & TRYGGVASON, G. 1990 The free-surface signature of unsteady, two-dimensional vortex flows, *J. Fluid Mech.* **218**, 547–572.